

# MaGICC Disks: Matching Observed Galaxy Relationships Over a Wide Stellar Mass Range

C. B. Brook<sup>1,2</sup>, G. Stinson<sup>3</sup>, B. K. Gibson<sup>2</sup>, J. Wadsley<sup>4</sup>, T. Quinn<sup>5</sup>

<sup>1</sup>*Departamento de Física Teórica, Universidad Autónoma de Madrid, E-28049 Cantoblanco, Madrid, Spain*

<sup>2</sup>*Jeremiah Horrocks Institute, University of Central Lancashire, Preston, PR1 2HE, UK*

<sup>3</sup>*Max-Planck-Institut für Astronomie, Königstuhl 17, 69117 Heidelberg, Germany*

<sup>4</sup>*Department of Physics and Astronomy, McMaster University, Hamilton, ON L8S 4M1, Canada*

<sup>5</sup>*Astronomy Department, University of Washington, Box 351580, Seattle, WA 98195-1580, USA*

## ABSTRACT

We use the same physical model to simulate four galaxies that match the relation between stellar and total mass, over a mass range that includes the vast majority of disc galaxies. The resultant galaxies, part of the Making Galaxies in a Cosmological Context (MaGICC) program, also match observed relations between luminosity, rotation velocity, size, colour, star formation rate, HI mass, baryonic mass, and metallicity. Radiation energy feedback from massive stars and supernova energy balance the complex interplay between cooling gas, regulated star formation, large scale outflows, and recycling of gas in a manner which correctly scales with the mass of the galaxy. Outflows, driven by the expansion of shells and superbubbles of overlapping supernova explosions, also play a key role in simulating galaxies with exponential surface brightness profiles, flat rotation curves and dark matter cores. Our study implies that large-scale outflows are the primary driver of the dependence of disc galaxy properties on mass. We show that the degree of outflows invoked in our model is required to meet the constraints provided by observations of OVI absorption lines in the circum-galactic media of nearby galaxies.

**Key words:** galaxies: evolution–galaxies: formation–galaxies: bulges galaxies: spiral

## 1 INTRODUCTION

The rotation velocity, size, luminosity (e.g. Courteau et al. 2007), star formation rate (e.g. Salim et al. 2007), stellar mass (e.g. Bell et al. 2003), total virial mass (including dark matter, Mandelbaum et al. e.g. 2006; More et al. e.g. 2011), mass of neutral hydrogen gas (e.g. Verheijen & Sancisi 2001), total baryon mass (e.g. McGaugh 2005) and the abundance of oxygen relative to hydrogen (e.g. Tremonti et al. 2004) are observationally well-determined. Together, the relation between these properties provide stringent constraints which simulations of galaxy formation must satisfy.

A large number of such disc galaxy properties vary with mass. Growing evidence suggests that the ratio of stellar mass to total mass of galaxies is low compared to the ratio of baryons to dark matter in the Universe. The relation is steep in the mass range where most disc galaxies exist, below a stellar mass  $\sim 2 \times 10^{10} M_{\odot}$ , where a doubling of halo mass results in a factor of eight more stellar mass. The relation has been determined by rank-ordering the masses of dark matter halos formed in simulations within the cold dark matter cosmological framework, and then

rank-ordering galaxies based on their stellar mass as determined in large scale galaxy surveys, and directly matching stellar and halo masses, assuming a monotonic relation between the two (Moster et al. 2010; Guo et al. 2010). The results agree remarkably well with direct derivations of the relation, where dark matter halo masses are determined by gravitational lensing (Mandelbaum et al. 2006) and the dynamics of satellite galaxies (More et al. 2011).

Recent progress in simulating galaxies in a cosmological cold dark matter framework has resulted in the ability to match an increasing number of properties of observed disk galaxies (Governato et al. 2010; Piontek & Steinmetz 2011; Agertz et al. 2011; Guedes et al. 2011) but have not been able to model the dependence of galaxy properties on mass.

Two approaches have emerged to regulate star formation in simulations. One method is to lower star formation efficiency either directly (Ageretz et al. 2011) or using small scale star formation physics based on the availability of molecular hydrogen ( $H_2$ ) from which stars form (Kuhlen et al. 2011). Agertz et al. (2011) produced a simulated galaxy which shares many features with the Milky Way, while (Kuhlen et al. 2011) produced low mass galaxies

at high redshift that match empirical star formation laws. Yet these models provide no mechanism to account for the steep decrease in stellar mass of galaxies found in lower mass galaxies, even accounting for the fact that lower mass galaxies have higher gas contents (e.g. Peebles & Shankar 2011).

A contrasting model invoking energy “feedback” from supernovae to regulate star formation has successfully simulated dwarf and Milky Way mass galaxies that share many properties of observed galaxies (Governato et al. 2010; Piontek & Steinmetz 2011; Guedes et al. 2011). Despite these successes, the galaxies simulated so far with the supernova energy feedback models form too many stars relative to their total mass (Sawala et al. 2011; Piontek & Steinmetz 2011; Avila-Reese et al. 2011), particularly in low mass simulations. Additionally, the simulations fail to match the specific star formation rates of observed galaxies (Colín et al. 2010; Avila-Reese et al. 2011).

In this paper we take the latter approach of directly injecting SNe energy. A clue to improving on such models came from measuring the velocity dispersion of the gas of our simulated dwarf galaxies, which was found to be significantly less turbulent than observed dwarf galaxies (Pilkington et al. 2011), suggesting that “feedback” energy has been under-estimated. Recent evidence suggests that radiative feedback from massive stars before they explode as supernovae can have significant effects in regulating star formation and adding energy to gas that surrounds newly forming clusters of stars (Nath & Silk 2009; Murray et al. 2011; Hopkins et al. 2011, 2012). Young, massive stars exert forces from their UV photons, stellar winds, and warm gas pressure from photo-ionized regions. In massive galaxies, momentum driven winds due to radiation pressure may be the primary driver of outflows (Murray et al. 2005; Hopkins et al. 2012). However, in galaxies of mass relevant to our study, the effect of the radiation feedback from massive stars is primarily to (i) prevent collapse of gas to small, dense regions, dissociating GMCs and regulating star formation, and (ii) stir up gas in star forming regions, punching holes that allow SNe remnants to expand and drive outflows (Hopkins et al. 2012), and (iii) provide pressure support in the disk.

Our model does not resolve this local radiation feedback from star forming regions nor individual supernovae, but it does resolve the shells and bubbles that are created by overlapping supernovae. Without the ability to resolve the details, we employ a relatively crude thermal implementation of radiation feedback from massive stars, with the aim being to mimic their most important effects on scales that we resolve, i.e. to regulate star formation, and enhance inhomogeneity in the ISM, creating turbulence that better matches observations, and to allow the expansion of the SNe driven super-bubbles which drive outflows.

Using this model, we simulate four galaxies with stellar masses ranging from  $2 \times 10^8$  to  $1.4 \times 10^{10} M_{\odot}$ . Crucially, the simulated galaxies (i) were run at the same resolution with identical input physics, and (ii) vary in their mass assembly history. Comparing the two most massive galaxies, SG3 has most of its merger activity at early times, prior to  $z = 2$ , whilst in SG4 significant merging activity occurs after  $z = 1$ . To illustrate the effect of feedback, we include results of SG1 using less feedback (SG1LF). It forms a galaxy with too many stars and is too compact. To study the way our model varies with resolution, we re-simulated SG3 at 8 times

lower resolution (SG1LR), run with the same feedback prescriptions, as well as a more massive galaxy SG5LR which extends the mass range of our sample out to  $3 \times 10^{10} M_{\odot}$ . These lower resolution simulated galaxies also match the scaling relations.

Section 2 describes the code and the initial conditions. Section 3 presents the basic properties of the simulations including star formation histories, rotation curves, radial light and dark matter density profiles. In Section 4 we show that the galaxies all fit on the observed relations between rotation velocity, size, luminosity, star formation rate, stellar mass, virial mass, HI mass, total baryon mass and metallicity. Section 5 shows that the outflows, which are central to our models, produce metal-enriched hot halos that reproduce the observed OVI column densities in the circum-galactic-medium (CGM, Prochaska et al. 2011; Tumlinson et al. 2011). In Section 6 we summarise our model for disc galaxy formation.

## 2 THE SIMULATIONS

### 2.1 The simulation code: GASOLINE

We have used **GASOLINE** (Wadsley et al. 2004), a fully parallel, N-Body+smoothed particle hydrodynamics (SPH) code, to compute the evolution of the collisionless and dissipative components in the simulations. The essential features of the code are outlined here.

Fluid elements representing gas are integrated using Smooth Particle Hydrodynamics (SPH, Gingold & Monaghan 1977; Monaghan 1992). **GASOLINE** is fully Lagrangian, spatially and temporally adaptive, and efficient for large  $N$ . Dissipation in shocks is modelled using the quadratic term of the standard Monaghan artificial viscosity (Monaghan 1992). The Balsara correction term is used to reduce unwanted shear viscosity. **GASOLINE** employs cooling due to H, He, and a variety of metal lines (Shen et al. 2010). The metal cooling grid is constructed using CLOUDY (version 07.02 Ferland et al. 1998), assuming ionisation equilibrium. A uniform ultraviolet ionising background (Haardt & Madau 1996) is used in order to calculate the metal cooling rates self-consistently. Two mechanisms are used to prevent gas from collapsing to higher densities than SPH can physically resolve: (i) to ensure that gas resolves the Jeans mass and does not artificially fragment, pressure is added to the gas in high density star forming regions (Robertson & Kravtsov 2008), (ii) a maximum density limit is imposed by setting a minimum SPH smoothing length of 0.25 times that of the gravitational softening length of  $\epsilon = 155$ pc. Each simulation has between 5-15 million particles within the virial radius at  $z = 0$ , with mean stellar particle mass of  $\sim 4800 M_{\odot}$  ( $\sim 38000 M_{\odot}$  in the low resolution runs).

### 2.2 The Initial Conditions

The simulations described here are cosmological zoom simulations derived from the McMaster Unbiased Galaxy Simulations (MUGS) (Stinson et al. 2010). Here, those initial conditions are scaled down, so that rather than residing in a 68 Mpc cube, it is inside a cube with 34 Mpc sides. This resizing

**Table 1.** Simulation data

| Name  | MUGS label | gas part. mass [ $M_{\odot}$ ] | IMF      | $c_{\star}$ | $M_{halo}$ [ $M_{\odot}$ ] | $M_{\star}$ [ $M_{\odot}$ ] | $M_R$ | $\mu_0^*$ | S*  | $n^{**}$ |
|-------|------------|--------------------------------|----------|-------------|----------------------------|-----------------------------|-------|-----------|-----|----------|
| SG1   | g5664      | $2.5 \times 10^4$              | Chabrier | 0.17        | $6.5 \times 10^{10}$       | $2.3 \times 10^8$           | -17.0 | 21.2      | 1.2 | 0.82     |
| SG2   | g1536      | $2.5 \times 10^4$              | Chabrier | 0.17        | $8.3 \times 10^{10}$       | $4.5 \times 10^8$           | -17.5 | 21.4      | 1.4 | 0.77     |
| SG3   | g15784     | $2.5 \times 10^4$              | Chabrier | 0.17        | $1.8 \times 10^{11}$       | $4.2 \times 10^9$           | -20.0 | 20.0      | 2.0 | 1.17     |
| SG4   | g157807    | $2.5 \times 10^4$              | Chabrier | 0.17        | $3.2 \times 10^{11}$       | $1.4 \times 10^{10}$        | -21.2 | 19.0      | 2.5 | 1.23     |
| SG1LF | g5664      | $2.5 \times 10^4$              | Kroupa   | 0.17        | $7.3 \times 10^{10}$       | $8.7 \times 10^9$           | -19.9 | 18.9      | 1.0 | 1.4      |
| SG3LR | g15784     | $2.0 \times 10^5$              | Chabrier | 0.33        | $1.8 \times 10^{11}$       | $4.6 \times 10^9$           | -20.1 | 19.9      | 2.1 | 1.1      |
| SG5LR | g1536      | $2.0 \times 10^5$              | Chabrier | 0.33        | $7.6 \times 10^{11}$       | $3.0 \times 10^{10}$        | -21.7 | 20.5      | 3.6 | 1.3      |

\*central surface brightness ( $\mu_0$ ), scale-lengths (size, S) and sersic indices ( $n$ ) from fits in the I band

\*\*SG1-4 and SGLR are single sersic fits, SG1LF and SG5LR are 2 component sersic bulge+exponential disk fits

allows us to compare galaxies with exactly the same merger histories at a variety of masses. Differences in the underlying power spectrum that result from this rescaling are minor (Springel et al. 2008; Macciò et al. 2008; Kannan et al. 2012), and do not effect our results. SG5LR is run with the original 68 Mpc cube, having the same initial conditions as SG3.

Table 1 shows the properties of the galaxies that were selected and rescaled from the MUGS sample. Note that SG3 uses the same initial conditions used in Brook et al. (2012), which showed the impact of galactic fountains on angular momentum distribution of galaxies. However, SG3 uses a different initial mass function (IMF) from (Brook et al. 2012), replacing Kroupa et al. (1993) with the more commonly used Chabrier (2003), which is more top heavy. The conclusions of Brook et al. (2012) remain valid in the new simulations.

### 2.3 Star Formation and Feedback

When gas reaches cool temperatures ( $T < 10,000$  K) in a dense environment ( $n_{th} > 9.3 \text{ cm}^{-3}$ ), it becomes eligible to form stars. This value for  $n_{th}$  is the maximum density gas can reach using gravity,  $32 \text{ m}_{gas}/\epsilon^3$ . Such gas is converted to stars according to the Schmidt Law:

$$\frac{\Delta M_{\star}}{\Delta t} = c_{\star} \frac{m_{gas}}{t_{dyn}} \quad (1)$$

where  $\Delta M_{\star}$  is the mass of the stars formed in  $\Delta t$ , the time between star formation events (0.8 Myrs in these simulations),  $m_{gas}$  is the mass of the gas particle,  $t_{dyn}$  is the gas particle's dynamical time and  $c_{\star}$  is the efficiency of star formation, in other words, the fraction of gas that will be converted into stars during  $t_{dyn}$ . Effective star formation rates are determined by the combination and interplay of  $c_{\star}$  and feedback, and so degeneracies do exist between feedback energy and the value of  $c_{\star}$ . In this study,  $c_{\star}$  is ultimately the free parameter that sets the balance of the baryon cycle off cooling gas, star formation, and gas heating. In our fiducial runs,  $c_{\star}=1.67\%$ .

Stars feed energy back into surrounding gas. Two types of energetic feedback are considered in these simulations, supernovae and early stellar radiation feedback from massive stars. Supernova feedback is implemented using the blast-wave formalism (Stinson et al. 2006) and deposits  $10^{51}$  erg of energy into the surrounding medium at the end of the stellar lifetime of every star more massive than  $8 M_{\odot}$ . Since

stars form from dense gas, the energy would be quickly radiated away due to the efficient cooling. For this reason, cooling is disabled for particles inside a blast region of size  $R = 10^{1.74} E_{51}^{0.32} n_0^{-0.16} \tilde{P}_{04}^{-0.20}$  pc and for the length of time  $t = 10^{6.85} E_{51}^{0.32} n_0^{0.34} \tilde{P}_{04}^{-0.70}$  yr. Here,  $E_{51} = 10^{51}$  erg,  $n_0$  is the ambient hydrogen density, and  $P_{04} = 10^{-4} P_0 k^{-1}$ , where  $P_0$  is the ambient pressure and  $k$  is the Boltzmann constant. Both  $n_0$  and  $P_0$  are calculated using the SPH kernel for the gas particles surrounding the star.

Metals are ejected from type II supernovae (SNII), type Ia supernovae (SNIa), and the stellar winds driven from asymptotic giant branch (AGB) stars. Ejected mass and metals are distributed to the nearest neighbour gas particles using the smoothing kernel (Stinson et al. 2006), using literature yields for SNII (Woosley & Weaver 1995) and SNIa (Nomoto et al. 1997). Metal diffusion is also included, such that unresolved turbulent mixing is treated as a shear-dependent diffusion term (Shen et al. 2010). This allows proximate gas particles to mix their metals. Metal cooling is calculated based on the diffused metals.

Radiation energy feedback from massive stars has been included in our model. To model the luminosity of stars, a simple fit of the mass-luminosity relationship observed in binary star systems by Torres (2010) is used:

$$\frac{L}{L_{\odot}} = \begin{cases} \left(\frac{M}{M_{\odot}}\right)^4, & M < 10M_{\odot} \\ 100\left(\frac{M}{M_{\odot}}\right)^2, & M > 10M_{\odot} \end{cases} \quad (2)$$

Typically, this relationship leads to  $2 \times 10^{50}$  ergs of energy being released from the high mass stars per  $M_{\odot}$  of the entire stellar population over the 4.5 Myr between the star's formation and the commencing of SNII. These photons do not couple efficiently with the surrounding ISM (Freyer et al. 2006). We thus do not want to couple all of this energy to the surrounding gas in the simulation. To mimic this highly inefficient energy coupling, we inject 10% of the energy as thermal energy in the surrounding gas, and cooling is *not* turned off for this form of energy input. It is well established that such thermal energy injection is highly inefficient at the spatial and temporal resolution of the type of cosmological simulations used here (Katz 1992; Kay et al. 2002). This is primarily due to the characteristic cooling timescales in the star forming regions being lower than the dynamical time.

In star forming regions where gas has density of  $\sim 10 \text{ cm}^{-3}$ , early stellar feedback typically heats the surrounding gas to between  $\sim 1$  to a few  $\times 10^6$  K. At the density where stars form in our simulations, i.e.  $n \sim 10 \text{ cm}^{-3}$ , cooling times are significantly shorter than dynamical times,

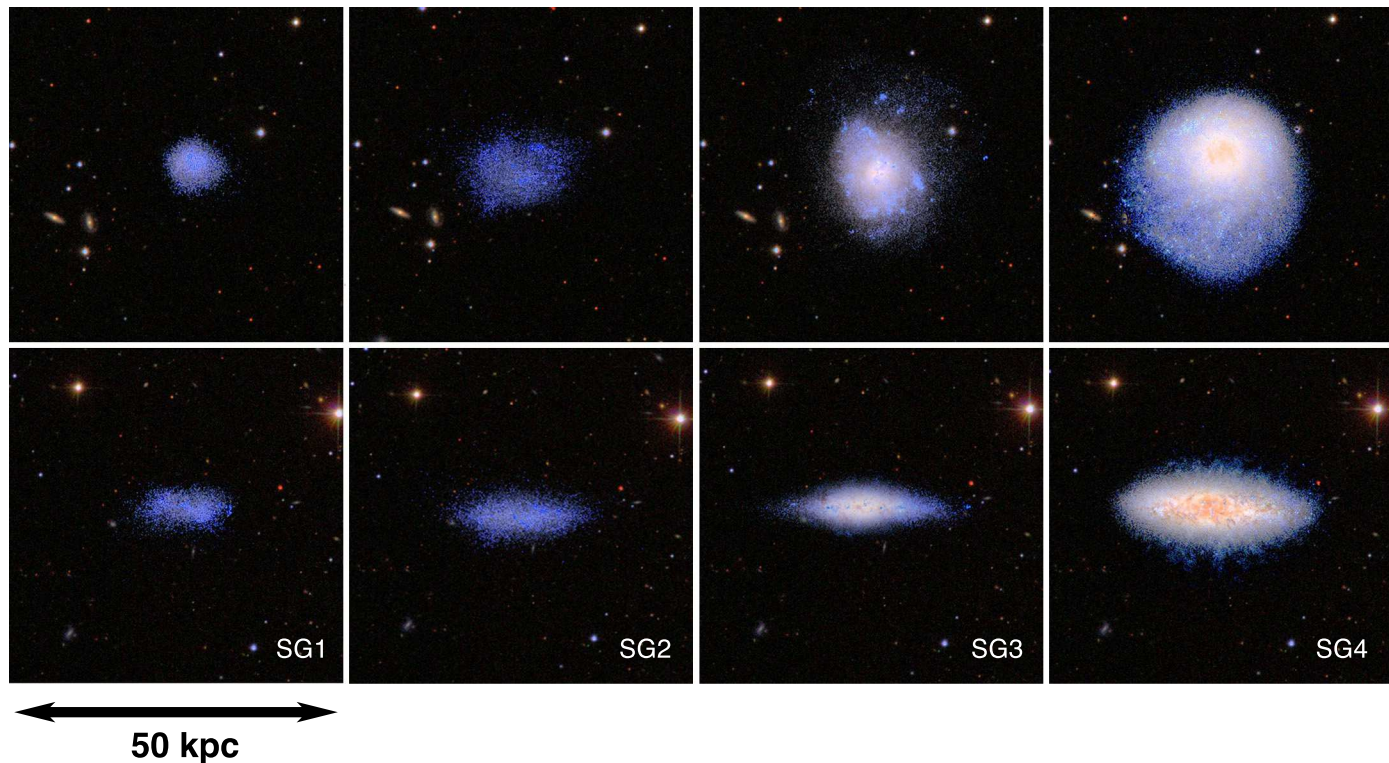


**Figure 1.** Mock images of the four simulated galaxies, made with SUNRISE (Jonsson 2006) that uses the ages and metallicities of simulated star particles, and the effects of dust reprocessing, to create stellar energy distributions. Filters which mimic Sloan Digital Sky Survey (SDSS) bands *i*, *r*, and *g*, are assigned to colours R, G, and B respectively to produce these images. The galaxies, from left to right, SG1, SG2, SG3 and SG4, are shown face-on (top panels) and edge-on (bottom panels). The significant asymmetry in SG4 is caused by the late accretion of a low mass satellite galaxy.

even for temperatures of order  $10^6\text{K}$  (see e.g. Figure 1 in Dalla Vecchia & Schaye 2012), typical of those which to our gas is heated by our radiation energy feedback, meaning that it is only gas particles which escape to less dense regions that have any effect from this feedback. We found that only  $\sim 10\%$  of heated particles had dynamical times longer than cooling times at high redshift ( $3 > z > 1$ ) when the ISM is most turbulent and the metallicity is low, reducing to only  $\sim 3\%$  by  $z = 0$ . Thus, between 90 – 97% is radiated away within a single dynamical time, meaning that our effective efficiency of coupling radiation energy feedback to the ISM is between 0.3–1%. It also means that our implementation does not evenly heat gas, i.e. we do not effectively couple the  $\lesssim 1\%$  of energy to all gas particles affected by radiation energy. Rather, our scheme is essentially stochastic, with a small number of gas particles effected. This scheme is thus somewhat similar to the SNe feedback implementation of Dalla Vecchia & Schaye (2012). This radiation energy feedback does not directly drive outflows: implemented in the absence of SNe feedback results in no outflows. Rather, it helps to regulate star formation, and enhances inhomogeneity in the ISM, creating increased turbulence, and allowing the expansion of the SNe driven super-bubbles which drive outflows.

To understand the effect of the strengthened feedback, a version of SG1 was simulated using the stellar feedback as implemented in Stinson et al. (2010) so that stars form when gas reached  $1\text{cm}^{-3}$ , with a Kroupa et al. (1993) IMF, with  $0.4 \times 10^{51}$  ergs deposited per supernova explosion. We

refer to this as the lower feedback model (LF) in this study, but note that this feedback strength is comparable to most implementations that are currently run in the literature (Scannapieco et al. 2011).

## 2.4 Resolution Dependence

To study the resolution dependence of our model, we also simulated two galaxies at  $8 \times$  lower resolution: SG3LR and SG5LR. Clearly, SG3LR is the low resolution version of SG3, while SG5LR is a galaxy with stellar (total) mass of  $3.0 \times 10^{10}$  ( $7.6 \times 10^{11}$ )  $M_{\odot}$ . As with other galaxy formation simulations in the literature, galaxy properties are not precisely the same at different resolutions when the same parameters are used (e.g. Scannapieco et al. 2011). In this study we aim to retain the same baryon cycle at the two different resolutions as this drives the simulated galaxy properties. Hence we want our star formation rates to match at the two resolutions. To achieve this we adjust our free parameter  $c_*$ , the input star formation efficiency, to ensure that the star formation rate remains the same at the two resolutions. With  $c_* = 0.033$ , SG3LR has a star formation rate that closely matches our fiducial high resolution run, SG3.

As the feedback implementation is the same between the two resolutions, the resultant galaxies have the same balance of star formation and feedback, and hence very similar baryon cycles, meaning that same key processes occur on the scales that we resolve i.e. the same the baryon cy-

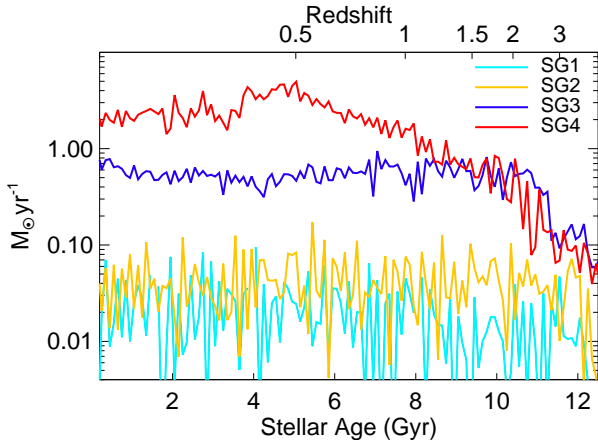


**Figure 2.** The star formation histories of the four simulated galaxies, SG1 (cyan line), SG2 (yellow), SG3 (blue), and SG4 (red). SG1 and SG2 have a bursty, yet reasonably consistent star formation histories. SG3 has a peak at high redshift, when it has its merging epoch, while SG4 has a much later merging epoch, resulting in a star formation rate that peaks at a later time.

cle between star formation, hot and cold gas, outflows and the density of gas in the star forming regions. At  $z=0$ , total baryon mass within the virial radius, the mass of stars, mass of hot gas ( $>4 \times 10^4 \text{K}$ ), and cold gas ( $<4 \times 10^4 \text{K}$ ) in SG3LR are all within 5-10% of the values for SG3. We will see that the resultant galaxies have almost identical properties with respect to scaling relations. We subsequently use the same calibration and input parameters for SG5LR, a more massive galaxy. This shows that we can form reasonable galaxies even at relatively low resolution, and it allows us to increase the range of masses over which our simulated galaxies match the scaling relations.

### 3 SIMULATED GALAXY CHARACTERISTICS

Mock observations of the four main simulated galaxies are shown in Figure 1. These images were created using the Monte Carlo radiative transfer code *SUNRISE* (Jonsson 2006), which simulates the effect of dust absorption. The morphologies of the galaxies range from dwarf irregular (SG1, SG2) to more structured disc galaxies (SG3, SG4). The significant asymmetry in SG4 is caused by the late accretion of a low mass satellite galaxy.

#### 3.1 Star Formation and Mass Accretion

Figure 2 shows the star formation histories of the simulated galaxies, SG1 (cyan line), SG2 (yellow), SG3 (blue) and SG4 (red). SG1 and SG2 both have bursty, yet reasonably consistent star formation histories. SG3 has a peak at high redshift, when it has its merging epoch, while SG4 has a much later merging epoch, resulting a star formation rate that peaks at a later time. The growth of the virial mass of the halos of the simulated galaxies is shown in Figure 3. Merger events appear as significant increases in the total mass. The later build-up of mass in SG4 relates directly to its later peak in star formation.

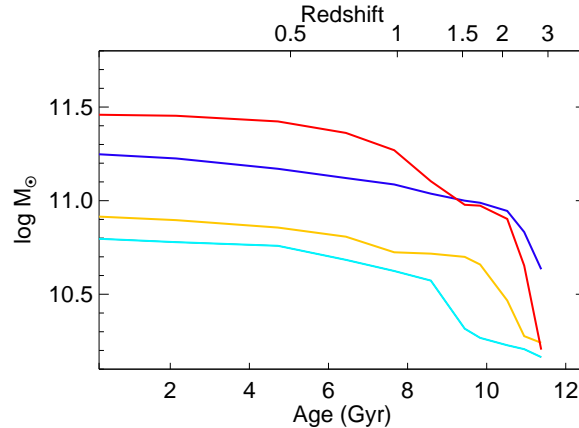


**Figure 3.** The growth of the virial mass of the halos of the simulated galaxies. The later build up of mass in SG4, which is still undergoing significant merging activity well after  $z=1$ , relates directly to its later peak in star formation.

#### 3.2 Surface Brightness Profiles

Figure 4 shows exponential (blue line) and single sersic (red line) fits to the I band profiles of the face-on surface brightness maps of each simulated galaxy, measured from face-on images and including the effects of dust reprocessing using *SUNRISE*. In each case we fit from the centre out to the radius where the I band surface brightness is  $25 \text{ M arcsec}^{-2}$ . The central surface brightness ( $\mu_0$ ), exponential scale-length ( $S$ ), and sersic index ( $n$ ) are shown. The values of scale-length ( $S$ ) are used for the “size” of the galaxy in this paper, to make consistent with the observational data with which comparison is made (Courteau et al. 2007). Each galaxy exhibits a nearly exponential surface brightness profile. In every case, the Sersic index,  $n < 1.5$ .

#### 3.3 Rotation Curves

Figure 5 shows the rotation curves of four main galaxies along with the low feedback version of SG1. The rotation velocities ( $V_c$ ) are computed by calculating the mass within spherical radial shells  $M(r)$ , then relating via  $V_c(r) = \sqrt{GM(r)/r}$  where  $G$  is Newton’s gravitational constant. Radial units are scaled by the disc scale-length in each case. The excessive central mass distribution that has plagued simulations of galaxy formation (Mayer et al. 2008) is absent in each case, reflected in the lack of central “peak” in the rotation curves. The vertical dotted and dashed lines are at 2.2 and 3.5 scale-lengths, where observational determinations of rotational velocity are often made (Courteau 1997; Giovanelli et al. 1997). We can see that in SG1, the rotation curve is still rising quite rapidly at 2.2 scale-lengths. This issue of rising rotation curves is also common in observations of low mass galaxies (Epinat et al. 2008). In this paper, we report the value of  $V_c$  at 3.5 scale-lengths in each case, as it best reflects the underlying mass of the system. Also shown is SG1LF, as a dashed cyan line. The contrast between the two SG1 galaxies is extreme, with much of the available baryons forming stars in the central region of the low feedback run, making the central region very dense and the rotation velocity very high in this region.

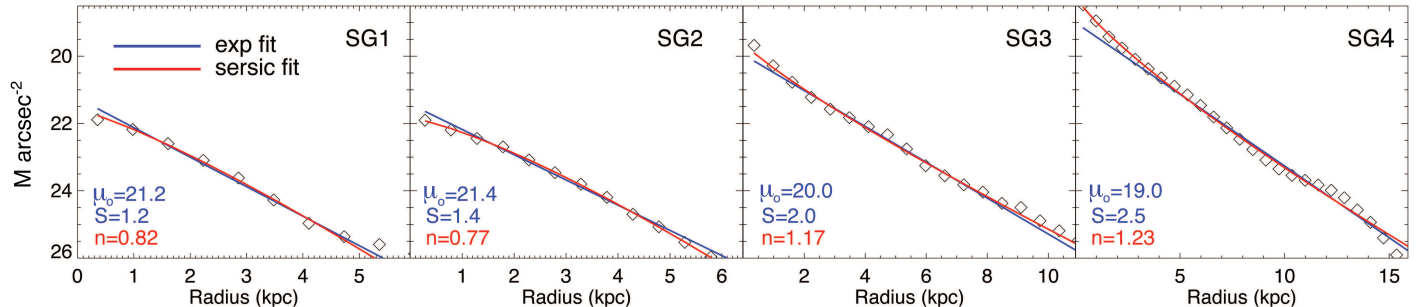


**Figure 4.** The I band surface brightness profiles of SG1, SG2, SG3 and SG4 from left to right respectively. Fits are made using both exponential (blue lines) and sersic (red lines) profiles. Central surface brightness ( $\mu_0$ ) and scale-lengths ( $S$ ) of the exponential fits as well as the sersic index ( $n$ ) from the sersic fits are noted in the bottom left of each panel. In each case fits are made from radius=0 out to  $I=25 \text{ M arcsec}^{-2}$ .

### 3.4 Dark Matter Profiles: Cores not Cusps

The dark matter density profile, on a log-log scale, is plotted for SG1 (cyan line), SG2 (yellow), SG3 (blue), and SG4 (red) in Figure 6. Also plotted is a dark matter only simulation of SG3, which has the steep inner profile that is characteristic of dark matter halos (Navarro et al. 1995). Radial units are scaled by the virial radius in each case. In all the simulated galaxies, the dark matter profile is less steep than the profiles in pure dark matter simulations. This flattening of the central dark matter profile when baryons are included has also been found in cosmological simulations of dwarf galaxies (Governato et al. 2010) and massive disc galaxies (Macciò et al. 2012). This contrasts with simulations that do not include strong feedback, which invariably have dark matter profiles that are even steeper than in pure dark matter simulations (Gnedin et al. 2011) because the dark matter adiabatically contracts as gas cools to the center. SG1LF (dashed cyan line) shows exactly this behaviour as its dark matter density profile is significantly steeper than the simulation that only includes dark matter. The fact that the amount of the outflows from the central region in the present study results in matching the scaling relations, favours the findings of simulations where “expansion” rather than contraction occurs over the masses of these simulations, as semi-analytic models have predicted (Dutton & van den Bosch 2009).

## 4 SCALING RELATIONS

The crucial test of galaxy formation models does not come from matching a single relation, as that can often be achieved through a parameter search of input physics. Rather, models are judged by their ability to simultaneously match a range of observational constraints.

### 4.1 Definitions

*Halo Mass:* To make a direct comparison to the abundance matching results, we use  $M_{200}$  from our dark matter only runs. As described in Stinson et al. (2010), one step in creating the initial conditions for the MUGS galaxies was running a zoom dark matter only simulation at the same resolution as the simulation that includes baryons.  $M_{200}$  is the mass

enclosed inside  $r_{200}$ , the radius at which the density reaches  $200\rho_c$ , where  $\rho_c$  is the critical density.

*Stellar Mass:* The sum of the mass of all stars within the radius where the I band surface brightness is  $25 \text{ M arcsec}^{-2}$ .

*HI mass:* The Saha equation is solved to determine an ionization equilibrium. This remains an approximation since an accurate model of HI mass would require full radiative transfer included in the code and is beyond the scope of this paper. In particular self shielding from the UV background is not included in our model and may result in our derived HI masses being under estimates, while photo-ionization of HI from the galaxy itself it also excluded.

*Cold gas mass:*  $4/3 \times M_{HI}(5h_r)$ . That is  $4/3$  the HI mass contained within five scale-lengths of the galaxy. A factor between 1.2 and 1.4 is commonly used in observations to account for heavy elements. We use  $4/3$  as it is used in the relevant observational studies to which we compare (McGaugh 2005).

*Magnitudes, luminosities and colours:* come directly from the **SUNRISE** outputs, and include the affects of dust reprocessing on the spectral energy distribution.

### 4.2 Relationships

Panel (a) of Figure 7 shows the relationship between the stellar mass and host halo mass of the four fiducial simulated galaxies as yellow diamonds, over-plotted on the published Guo et al. (2010) relationship. Our free parameter,  $c_*$ , was tuned to place SG3 on this relationship. There was no guarantee that the other simulated galaxies should fall on this relationship. The red triangle represents the low feedback case, SG1LF, which demonstrates that low feedback results in more than an order of magnitude too many stars.

The green diamonds represents the low resolution runs. As stated, we adjusted  $c_*$  such that the star formation rate in SG3LR matched as closely as possible to that of SG3. As we have not changed our feedback recipe, the balance between star formation and energy feedback remains the same at the two resolutions. What is interesting is that using these parameters for a more massive galaxy, SG5LR, the simulation again fits on the relation, extending the mass range over which our balance between star formation and feedback results in the correct scaling of stellar mass with

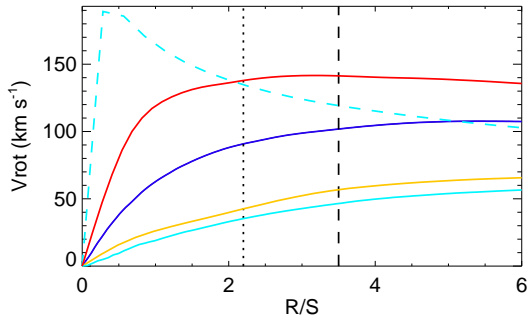


**Figure 5.** Rotation velocity ( $V_c$ ) versus radius of SG1 (cyan line), SG2 (yellow), SG3 (blue) and SG4 (red). Radial units are scaled by the disc scale-length in each case. The low feedback simulation, SG1LF (dashed cyan line) shows the extreme difference in stars formed compared to the fiducial run, particularly in the central regions, combined with adiabatic contraction rather than expansion. The dotted and dashed vertical lines are at 2.2 and 3.5 scale-lengths. In the paper, we use  $V_c$  as measured at 3.5 scale-lengths in each case, as it better reflects the underlying mass of the system.

halo mass. A more thorough analysis of SG5LR will be made in a forthcoming study.

Figures 7 & 8 show the relationships between the rotation velocity, size, luminosity, star formation rate stellar mass, total mass, HI mass, total baryon mass and metallicity of the simulated disc galaxies. The fiducial simulations match the relations remarkably, and their properties correctly scale over the mass range of the simulations. Again, we emphasise that none of the parameters were tuned in order to match any of these relations. As stated, the only tuning was to adjust  $c_*$  such that SG3 (and SG3LR) fits on the stellar mass-halo mass relation. The low resolution cases (green diamonds) also match the relations, with SG3LR matching well its high resolution counterpart.

It is very interesting that the thermal feedback implementation results in stellar mass-halo mass relation that has such steep dependence on mass (panel 7a). Our feedback has no mass dependence nor mass loading included in its implementation. It simply inputs a given amount of energy per unit of star formation, resulting in pressure from thermal energy that drives outflows, controlling the supply of cold gas available for star formation. Feedback processes then further regulate the star formation rates of this cold gas.

The other panels in Figure 7 (b-d) relate to the angular momentum of the galaxies at given luminosities. Matching the Tully-Fisher relation over a wide range in luminosities, combined with making disk galaxies of the correct size (without large stellar bulges), indicates that we have attained the correct amount and distribution of angular momentum. The angular momentum of the baryons in these simulations do not simply follow the dark matter, as analytic models often assume. Rather, the distributions arise from a cycle of cooling to the star forming regions, outflows, and galactic fountains (see Brook et al. 2011, 2012).

The relations in Figure 8 put further constraints on the baryon cycle of galaxies of varying mass. Even though our feedback drives outflows, it does not simply eject all the cold gas from the disk. This is the result of the inhomogeneous in-

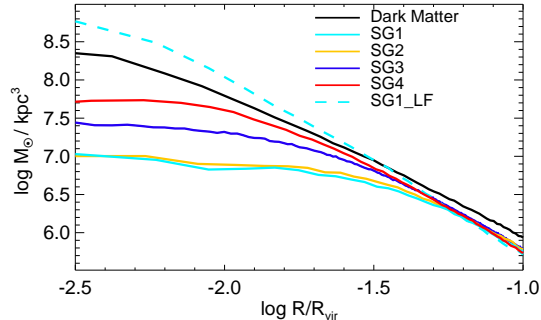


**Figure 6.** The dark matter density profiles, on a log-log scale, where radial units are scaled by the virial radius. Also plotted is a dark matter only simulation of SG3, which has the steep inner profile that is characteristic of dark matter halos. The low feedback simulation SG1LF (dashed cyan line) shows significant adiabatic contraction.

terstellar medium, with pockets of hot gas building pressure and driving outflows. This is key in allowing the high HI fractions in the low mass galaxies (Panel 8c), even though they lose a high fraction of their baryons in the outflows. These processes also relate directly to the success of the low mass simulations in matching the specific star formation rates. Simulations have largely had trouble matching the specific star formation rate for low mass galaxies (Colin et al. 2010; Avila-Reese et al. 2011). With low feedback, the star formation rates follow the gas accretion rates, which exponentially decline after  $z \sim 2$ , meaning that the stars form too early. Attempts to form significantly fewer stars in dwarf galaxies by increasing feedback had the trouble of ejecting their gas in high redshift star bursts, resulting in isolated dwarf spheroidal galaxies (Sawala et al. 2010), rather than dwarfs with prolonged star formation histories and significant amounts of HI gas at  $z = 0$ , as observed in the field (e.g. Geha et al. 2006). Our feedback implementation is able to maintain significant amounts of cold gas in the star forming region, to regulate star formation whilst driving outflows and gas recycling via galactic fountains.

The match to the baryonic mass-metallicity relation (panel 8d) provides added confidence in the baryon cycle that our feedback creates. The balance between fresh gas accretion, metal injection from star forming regions, metal enriched outflows and recycling conspires to result in the correct gas metallicities at each mass range. We show in Section 5 that this cycle of metals also results in OVI abundances in the circum-galactic medium (CGM) that match observations. Further detailed studies of the metallicities and their distributions will be made in forthcoming studies, placing greater constraints on our baryon cycle.

The low feedback case (SG1LF) is also particularly interesting. The huge increase in number of stars formed means much more mass in the inner region, so the rotation velocity (measured at 3.5 scale-lengths) is much higher than in the high feedback case. Yet the increased stellar mass also results in higher luminosity: the values conspire so that it remains on the Tully-Fisher relation. Of course, the peaked rotation curve means a there is dependence on the radius at which rotation is measured. Beyond the mass-metallicity relation, it requires the size-metallicity relation to break the

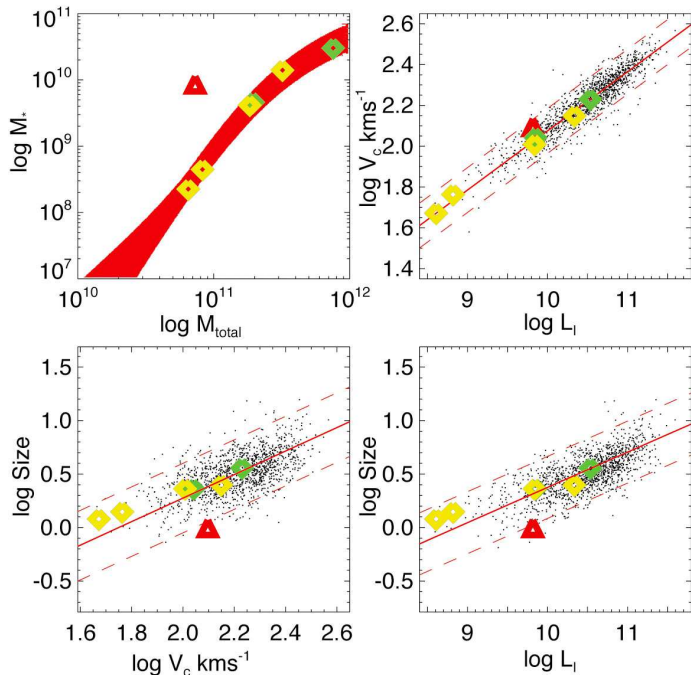


**Figure 7.** Scaling relations of the simulated galaxies overplotted on observational data. All plots are shown on a log scale. Panel (a) Stellar mass ( $M_*$ ) against total mass ( $M_{\text{vir}}$ ). The thick red line shows the (semi) empirical relation (Sawala et al. 2011). All other plots use a single observational data set (Courteau et al. 2007). Red lines are fits to the observational data while dashed red lines include 97% of data. Panel (b) Rotational velocity ( $V_c$ ) against Luminosity ( $L_I$ ) in the I-band (the Tully-Fisher relation). Panel (c) Size ( $S$ ), or disc scale-length, against  $L_I$ . Panel (d)  $S$  against  $V_c$ . The four fiducial runs are shown as yellow diamonds, the low resolution runs as green diamonds and the low feedback run as a red triangle.

degeneracy of the high and low feedback cases both fitting on the Tully-Fisher relation. The low feedback run is too concentrated. Thus the shape of the rotation curve and the three parameters size-luminosity-rotation are required to assess simulations. This was pointed out in Dutton & Courteau (2008). The low feedback run is also deficient in HI relative to its R-band luminosity (panel 8c), due to turning too much of its cold gas into stars.

## 5 METAL ENRICHED GASEOUS CORONA

One way to test the extent of outflows, and hence the feedback in our model, is to compare the metal enriched gas surrounding the simulated galaxies with observations. Prochaska et al. (2011) and Tumlinson et al. (2011) find that column densities of OVI extend out to 300 kpc from star forming galaxies. Their observations extend to galaxies as faint as  $0.01 L^*$ , making them especially useful to compare with our models. Figure 9 shows the surface density profiles of OVI gas as a function of the impact parameter,  $\rho$ , from the centre of the simulated galaxies. The observed OVI column densities for sub- $L^*$  galaxies at  $z \sim 0$  from (Prochaska et al. 2011, blue dots) and (Tumlinson et al. 2011, green dots) are shown overplotted on the model data. Each panel is labeled with the V-band luminosity of the simulated galaxies and

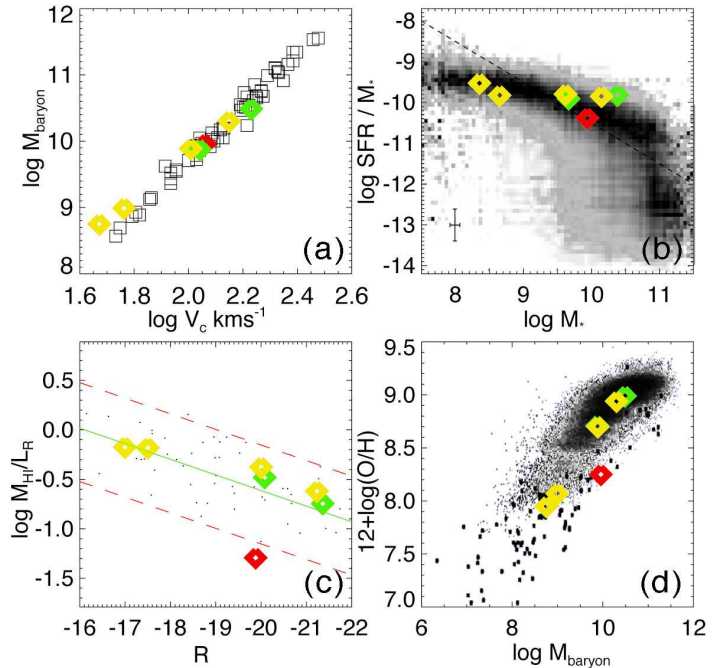


**Figure 8.** Simulated galaxies overplotted on observational data. Panel (a) Total baryonic mass ( $M_{\text{baryon}}$ ), consisting of all stars and cold gas, plotted against  $V_c$  (observed data from McGaugh 2005). Panel (b) Specific star formation rate against stellar mass (observed data from Salim et al. 2007). Panel (c) The ratio of the mass of neutral hydrogen gas (HI) to luminosity in the R-band ( $L_R$ ) plotted against the R-band magnitude (observed data from Verheijen & Sancisi 2001). Red lines are fits to the observational data while dashed red lines include 97% of data. Panel (d) The ratio of Oxygen to Hydrogen,  $12+\log(\text{O}/\text{H})$ , against total baryonic mass (observed data from Tremonti et al. 2004). The four fiducial runs are shown as yellow diamonds, the low resolution runs as green diamonds and the low feedback run as a red triangle.

the virial radius, indicated by the vertical green lines. Our feedback implementation produces extended, metal enriched gaseous coronae that extend to impact parameters of  $\sim 300$  kpc, even around low mass halos, matching observed absorption line features. We refer the reader to Stinson et al. (2011) which presents full details of our comparisons between simulations and observations and shows that the low feedback case is significantly deficient in OVI within its CGM. Note that the affects of metal diffusion on the distribution of metals were explored in Shen et al. (2010) and they find that the effect is minimal these results.

## 6 CONCLUSIONS

We use the same physical model, including feedback implementation, at the same resolution to simulate four galaxies over a wide mass range that match a range of galaxy properties and scaling relations. Our model includes radiation energy from massive stars, as well as supernova energy. We adjusted the star formation efficiency parameter  $c_*$  so that a single simulated galaxy, SG3, matched the stellar mass-halo mass relation (Moster et al. 2010; Guo et al. 2010). With the additional energy sources driving outflows from star formation regions in our updated model, the complex interplay



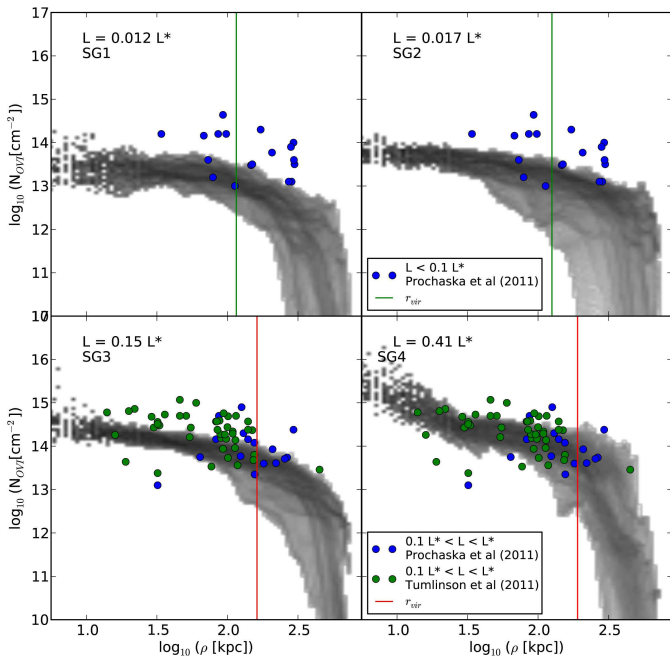


**Figure 9.** Radial profiles of the column density maps of OVI for the 4 simulated galaxies. The large dots are observations of  $L < 0.1 L_*$  galaxies from Prochaska et al. (2011) (blue, top panels) and in the lower panels the  $0.1 L_* < L < L_*$  galaxies from Prochaska et al. (2011, blue) and Tumlinson et al. (2011, green) galaxy samples. The solid vertical green (red) line represents the virial radius in the upper (lower) panels for each of the four halos.

between cooling gas, star formation, radiation energy injection from massive stars, stellar winds and supernova explosions, outflows, and the recycling of gas (the baryon cycle) have been balanced in our model to (i) retain the correct amount of baryons, blowing out large amounts of gas from the central regions, particularly in low mass galaxies, (ii) reproduce star formation rates and histories to attain the correct galaxy luminosities, stellar masses and colours for a given mass galaxy, (iii) ensure that low mass galaxies are gas rich compared to high mass galaxies, relative to their stellar population, even though significantly more gas is blown out of the low mass galaxies, (iv) attain an amount and distribution of angular momentum in the star forming gas to result in the correct morphology and disc sizes, and (v) correctly balance inflows of fresh gas with the recycling of gas from star forming regions, in order to correctly match the mass-metallicity relation.

We have previously shown that the outflows in our model remove low angular momentum gas (Brook et al. 2011), resolving the “angular momentum problem” which has plagued simulations (e.g. Navarro & Steinmetz 2000; Piontek & Steinmetz 2011). Some of the heated gas is ejected from the galaxy entirely, particularly at early times and from the low mass galaxies, while some of the gas is blown only as far as the dark matter halo that surrounds the galaxy, and may cool back down to the star forming region at later times and form disc stars (Brook et al. 2012). In our four simulated disc galaxies, outflows from the central regions also drive an expansion of the central dark matter

profiles, resulting in flat dark matter central density profiles which better match observed galaxies, rather than the very steep density profile that are predicted from dark matter simulations even in our most massive disc galaxy simulation.

By re-calibrating the input star formation efficiency in order to attain the same star formation rate in a lower resolution simulation (SG3LR) as in the fiducial run (SG3) without changing the feedback implementation, we were able to attain a very similar baryon cycle and hence a galaxy with very similar properties at two resolutions. Our calibration for this lower resolution also resulted in an  $L_*$  galaxy (SG5LR) that matches the scaling relations. By contrast, a low feedback run (SG1LF) was shown to form too many stars, particularly in the central regions. Our study shows that it is necessary to examine a number of relations to determine the success of simulations, and we recommend plotting at minimum the size-luminosity-rotation velocity properties rather than simply the Tully-Fisher relation (see also Dutton & Courteau 2008).

Our model suggests that large scale outflows of gas from the central regions of galaxies are the primary driver of galaxy scaling relations, as well as shaping disc morphology. The model makes the assumption that radiation energy from massive stars regulates star formation and stir up gas in star forming regions, allowing SNe remnants to expand and drive outflows. We show that the scale of outflows invoked in our models matches the observed absorption line features of local galaxies (Prochaska et al. 2011; Tumlinson et al. 2011). A detailed comparison between the simulations and these observations is made in Stinson et al. (2011), where we show that lower feedback models, more akin to those commonly used (e.g. Scannapieco et al. 2011), are significantly deficient in extended OVI, particularly in low mass galaxies.

Only in a very narrow mass range does the gravitation of host dark matter halos balance the processes causing these outflows, allowing disc galaxies to form. In the lower mass halos, the significant energy feedback drives increased turbulence, leading to more irregular galaxy morphologies (SG1, SG2).

## ACKNOWLEDGMENTS

CB and BKG acknowledge the support of the UKs Science & Technology Facilities Council (STFC Grant ST/F002432/1). TQ was supported by NSF grant AST- 0908499. We acknowledge the computational support provided by the UKs National Cosmology Supercomputer, COSMOS.

## REFERENCES

- Agertz O., Teyssier R., Moore B., 2011, MNRAS, 410, 1391
- Avila-Reese V., Colín P., González-Samaniego A., Valenzuela O., Firmani C., Velázquez H., Ceverino D., 2011, ArXiv e-prints
- Bell E. F., McIntosh D. H., Katz N., Weinberg M. D., 2003, ApJL, 585, L117
- Brook C. B., Governato F., Roškar R., Stinson G., Brooks A. M., Wadsley J., Quinn T., Gibson B. K., Snaith O.,

- Pilkington K., House E., Pontzen A., 2011, *MNRAS*, pp 595–+
- Brook C. B., Stinson G., Gibson B. K., Roškar R., Wadsley J., Quinn T., 2012, *MNRAS*, 419, 771
- Chabrier G., 2003, *ApJL*, 586, L133
- Colín P., Avila-Reese V., Vázquez-Semadeni E., Valenzuela O., Ceverino D., 2010, *ApJ*, 713, 535
- Courteau S., 1997, *AJ*, 114, 2402
- Courteau S., Dutton A. A., van den Bosch F. C., MacArthur L. A., Dekel A., McIntosh D. H., Dale D. A., 2007, *ApJ*, 671, 203
- Dalla Vecchia C., Schaye J., 2012, *ArXiv e-prints*
- Dutton A. A., Courteau S., 2008, in Funes J. G., Corsini E. M., eds, *Formation and Evolution of Galaxy Disks* Vol. 396 of *Astronomical Society of the Pacific Conference Series*, *Confronting Scaling Relations of Spiral Galaxies with Hierarchical Models of Disk Formation*. p. 463
- Dutton A. A., van den Bosch F. C., 2009, *MNRAS*, 396, 141
- Epinat B., Amram P., Marcelin M., 2008, *MNRAS*, 390, 466
- Ferland G. J., Korista K. T., Verner D. A., Ferguson J. W., Kingdon J. B., Verner E. M., 1998, *PASP*, 110, 761
- Freyer T., Hensler G., Yorke H. W., 2006, *ApJ*, 638, 262
- Geha M., Blanton M. R., Masjedi M., West A. A., 2006, *ApJ*, 653, 240
- Gingold R. A., Monaghan J. J., 1977, *MNRAS*, 181, 375
- Giovanelli R., Haynes M. P., Herter T., Vogt N. P., da Costa L. N., Freudling W., Salzer J. J., Wegner G., 1997, *AJ*, 113, 53
- Gnedin O. Y., Ceverino D., Gnedin N. Y., Klypin A. A., Kravtsov A. V., Levine R., Nagai D., Yepes G., 2011, *ArXiv e-prints*
- Governato F., Brook C., Mayer L., Brooks A., Rhee G., Wadsley J., Jonsson P., Willman B., Stinson G., Quinn T., Madau P., 2010, *Nature*, 463, 203
- Guedes J., Callegari S., Madau P., Mayer L., 2011, *ApJ*, 742, 76
- Guo Q., White S., Li C., Boylan-Kolchin M., 2010, *MNRAS*, 404, 1111
- Haardt F., Madau P., 1996, *ApJ*, 461, 20
- Hopkins P. F., Quataert E., Murray N., 2011, *ArXiv e-prints*
- Hopkins P. F., Quataert E., Murray N., 2012, *MNRAS*, 421, 3522
- Jonsson P., 2006, *MNRAS*, 372, 2
- Kannan R., Macciò A. V., Pasquali A., Moster B. P., Walter F., 2012, *ApJ*, 746, 10
- Katz N., 1992, *ApJ*, 391, 502
- Kay S. T., Pearce F. R., Frenk C. S., Jenkins A., 2002, *MNRAS*, 330, 113
- Kroupa P., Tout C. A., Gilmore G., 1993, *MNRAS*, 262, 545
- Kuhlen M., Krumholz M., Madau P., Smith B., Wise J., 2011, *ArXiv e-prints*
- Macciò A. V., Dutton A. A., van den Bosch F. C., 2008, *MNRAS*, 391, 1940
- Macciò A. V., Stinson G., Brook C. B., Wadsley J., Couchman H. M. P., Shen S., Gibson B. K., Quinn T., 2012, *ApJL*, 744, L9
- Mandelbaum R., Seljak U., Kauffmann G., Hirata C. M., Brinkmann J., 2006, *MNRAS*, 368, 715
- Mayer L., Governato F., Kaufmann T., 2008, *Advanced Science Letters*, 1, 7
- McGaugh S. S., 2005, *ApJ*, 632, 859
- Monaghan J. J., 1992, *ARAA*, 30, 543
- More S., van den Bosch F. C., Cacciato M., Skibba R., Mo H. J., Yang X., 2011, *MNRAS*, 410, 210
- Moster B. P., Somerville R. S., Maulbetsch C., van den Bosch F. C., Macciò A. V., Naab T., Oser L., 2010, *ApJ*, 710, 903
- Murray N., Ménard B., Thompson T. A., 2011, *ApJ*, 735, 66
- Murray N., Quataert E., Thompson T. A., 2005, *ApJ*, 618, 569
- Nath B. B., Silk J., 2009, *MNRAS*, 396, L90
- Navarro J. F., Frenk C. S., White S. D. M., 1995, *MNRAS*, 275, 56
- Navarro J. F., Steinmetz M., 2000, *ApJ*, 538, 477
- Nomoto K., Iwamoto K., Nakasato N., Thielemann F.-K., Brachwitz F., Tsujimoto T., Kubo Y., Kishimoto N., 1997, *Nuclear Physics A*, 621, 467
- Peeples M. S., Shankar F., 2011, *MNRAS*, 417, 2962
- Pilkington K., Gibson B. K., Calura F., Brooks A. M., Mayer L., Brook C. B., Stinson G. S., Thacker R. J., Few C. G., Cunnama D., Wadsley J., 2011, *MNRAS*, 417, 2891
- Piontek F., Steinmetz M., 2011, *MNRAS*, 410, 2625
- Prochaska J. X., Weiner B., Chen H.-W., Mulchaey J., Cooksey K., 2011, *ApJ*, 740, 91
- Robertson B. E., Kravtsov A. V., 2008, *ApJ*, 680, 1083
- Salim S., Rich R. M., Charlot S., Brinchmann J., Johnson B. D., Schiminovich D., Seibert M., Mallery R., Heckman T. M., Forster K., Friedman P. G., 2007, *ApJS*, 173, 267
- Sawala T., Guo Q., Scannapieco C., Jenkins A., White S., 2011, *MNRAS*, 413, 659
- Sawala T., Scannapieco C., Maio U., White S., 2010, *MNRAS*, 402, 1599
- Scannapieco C., Wadepuhl M., Parry O. H., Navarro J. F., Jenkins A., Springel V., Teyssier R., Schaye J., Stinson G. S., Theuns T., Wadsley J., White S. D. M., Woods R., 2011, *ArXiv e-prints*
- Shen S., Wadsley J., Stinson G., 2010, *MNRAS*, 407, 1581
- Springel V., Wang J., Vogelsberger M., Ludlow A., Jenkins A., Helmi A., Navarro J. F., Frenk C. S., White S. D. M., 2008, *MNRAS*, 391, 1685
- Stinson G., Brook C., Prochaska J. X., Hennawi J., Pontzen A., Shen S., Wadsley J., Couchman H., Quinn T., Macciò A. V., Gibson B. K., 2011, *ArXiv e-prints*
- Stinson G., Seth A., Katz N., Wadsley J., Governato F., Quinn T., 2006, *MNRAS*, 373, 1074
- Stinson G. S., Bailin J., Couchman H., Wadsley J., Shen S., Nickerson S., Brook C., Quinn T., 2010, *MNRAS*, 408, 812
- Torres G., 2010, *AJ*, 140, 1158
- Tremonti C. A., Heckman T. M., Kauffmann G., Brinchmann J., Charlot S., White S. D. M., Seibert M., Peng E. W., Schlegel D. J., Uomoto A., Fukugita M., Brinkmann J., 2004, *ApJ*, 613, 898
- Tumlinson J., Thom C., Werk J. K., Prochaska J. X., Tripp T. M., Weinberg D. H., Peeples M. S., O'Meara J. M., Oppenheimer B. D., Meiring J. D., Katz N. S., Davé R., Ford A. B., Sembach K. R., 2011, *Science*, 334, 948
- Verheijen M. A. W., Sancisi R., 2001, *AAP*, 370, 765
- Wadsley J. W., Stadel J., Quinn T., 2004, *New Astronomy*,

9, 137

Woosley S. E., Weaver T. A., 1995, ApJS, 101, 181